Supplementary Information

Universal strategy of capacity-compensation via electrolyte for Li-ion batteries

Xiaoyi Wang[1], Shaojie Zhang[1], Yu Cao[1,2], Haochen Gong[1], Mengting Zheng[3], Jun Lu[3, *], Jie Sun[1,2,4,5, *]

[1] School of Chemical Engineering and Technology, Tianjin University, Tianjin, 300350, China

[2] Quzhou Institute for Innovation in Resource Chemical Engineering, No. 78, Jiuhuabei Avenue, Zhejiang, 324000, China

[3] College of Chemical and Biological Engineering, Zhejiang University, Hangzhou, 310027, China

[4] School of Materials Science and Engineering, Nankai University, Tianjin 300350, China.

[5] National institute for advanced materials, Nankai university, Tianjin 300350, P. R. China

*Corresponding author. E-mail: jies@tju.edu.cn; junzoelu@zju.edu.cn

Supplementary Tables and Figures

Discussion of the difference between Li_5FeO_4 and Li_xPPs

1) **Cost**: The price of raw materials for preparing LiP_7: the price of LiP_7 is approximately \$6287/ton. As for the preparation of Li_5FeO_4, the price is approximately \$7783/ton. What's more, Li_5FeO_4 faces the problem of incomplete release of lithium ions which causes high cost. Therefore, less LiP_7 is needed to compensate for the initial capacity loss and the cost of Li_xPPs is lower than the traditional prelithiation reagents.

2) **Compatibility**: Firstly, the extremely poor air stability makes it difficult for Li_5FeO_4 to be mass-produced and applied in engineering practice. When handling or storing Li_5FeO_4 in an air environment, noticeable capacity losses occur, which might be caused by the residual Li species (such as Li_2O, LiOH, or Li_2CO_3). These byproducts will further result in high interfacial resistance and poor kinetic performance on the surface (*Adv. Funct. Mater. 2024, 34, 2315010)*. In industrial applications, it is usually necessary to encapsulate conductive carbon materials on the surface of Li_5FeO_4 at high temperatures to improve its electronic conductivity and environmental resistance (*Adv. Funct. Mater. 2024, 34, 2315010*). In contrast, Li_xPPs can be dissolved in the electrolyte and be added to the battery cell through the injection process, thus its compatibility with air can be neglected.

Secondly, Li_5FeO_4 is not compatible with all kinds of battery systems. Li_5FeO_4 is mixed in the slurry of the cathode, but the residual Li species would easily lead to the increase of alkalinity in the cathode slurry, defluorination of the PVDF binder, and slurry gelation, all of which deteriorate the mechanical properties. These damages to the cathode slurry demonstrate that Li_5FeO_4 does not meet the practical manufacturing requirements for Ni-rich layered oxide cathodes (*Adv. Energy Mater. 2023, 13, 2300507*). To address the above issues, we proposed the capacity-compensation method through electrolyte, which has no negative effect on the electrodes. What's more, Li_xPPs is also able to form a thin and stable CEI that will effectively maintain the stability of the cathode (**Fig. 5**).

3) **Safety**: During the first charging process, Li_5FeO_4 undergoes an irreversible phase transformation from antifluorite structure (belonging to *Pbca* space group) to a disordered rock salt phase ($LiFeO_2$), accompanied by the production of a large amount of O_2, which pose a threat to the safety of cathode (*Adv. Funct. Mater. 2024, 34, 2315010)*. As for Li_xPPs, its decomposition products are solid phosphates and P^0, which can be adhered to the surface of the cathode and act as a fire retardant. Consequently, the safety of the battery

is enhanced.

4) **Battery life**: Li_5FeO_4 undergoes volume shrinkage after the delithiation process, which will affect the cycling stability of the battery. As for Li_xPPs, it is not involved in the electrode originally, thus it will not create cavities in the electrode. For example, the NCM811||graphite full-cell with Li_5FeO_4 only shows a reversible capacity of 98.5 mAh g^{-1} after 50 cycles (*Adv. Funct. Mater. 2024, 34, 2315010)*, which is significantly lower than the 171.7 mAh g^{-1} after 400 cycles in this work (**Fig. 3c**).

5) **Operability**: Firstly, as discussed in the "compatibility" part, residual Li species (such as Li_2O, LiOH, or Li_2CO_3) exist at the surface of Li_5FeO_4. During the electrode pretreatment, the cathode materials are under threat from the residuals. In addition, Li_5FeO_4 has to be stored in Ar atmosphere, leading to additional operation and extra costs. Li_xPPs is able to be stored in electrolyte, implying that neither additional steps nor equipment are required. The capacity-compensation through electrolyte exhibits higher operational feasibility.

Secondly, the preparation of Li_5FeO_4 requires high-temperature calcination. For example, Su et al. mixed LiOH-H_2O and Fe_2O_3 as the starting material (*J. Power Sources, 2016, 324, 150-157)*. The preparation process of Li_5FeO_4 involves multiple steps and high-temperature calcination, which is relatively cumbersome. The preparation of Li_xPPs in this article only needs to add Li and red phosphorus to Li-biphenyl solution and stir at room temperature overnight, thus there is no need for high temperature, and the preparation process is facile.

6) **Capacity**: The specific capacity of LiP_7 (4307 mAh g^{-1}) is significantly higher than that of Li_5FeO_4 (867 mAh g^{-1}).

Supplementary Table S1 The mechanism of various cathode prelithiation reagents and Li_xPPs (this work).

Prelithiation reagent		Prelithiation mechanism	Decomposition voltage(V)	Specific capacity (mAh g^{-1})
Li-rich ternary compounds	Li_2NiO_2	$Li_2NiO_2 \rightarrow Li_{1-x}NiO_2 + xLi^+ + xe^-$	1.75	300
	Li_5FeO_4	$Li_5FeO_4 \rightarrow LiFeO_2 + O_2\uparrow + 4Li^+ + 4e^-$	3.5	700
	Li_6CoO_4	$Li_6CoO_4 \rightarrow Li_{6-x}CoO_y + xLi^+ + (4-y)/2\ O_2 + xe-$, $y = 4-(x-2)/2$	3.4	1167
LiX/M (X = F, O, S, M= metal)	Li_2S/M	$4Li_2S + 3Fe^0 \rightarrow Fe_3S_4 + 8Li^+ + 8e^-$	2.5	700
	LiF/M	$3LiF+Co \rightarrow CoF3 + 3Li^+ + 3e^-$	3.2	550
	Li_2O/M	$4Li_2O + 3Fe^0 \rightarrow Fe_3O_4 + 8Li^+ + 8e^-$	2	650
Li-rich binary compounds	Li_2S	$Li_2S \rightarrow 2Li^+ + 2\ e^- + S$	2.5	1167
	Li_3N	$2Li_3N \rightarrow 6Li^+ + 6\ e^- + N_2\uparrow$	0.9 (pure)/ 4.3(passivated)	2309
Li_xPPs	LiP_7	$LiP_7 + 28\ O^{2-} \rightarrow 7PO_4^{3-} + Li^+ + 36\ e^-$	3.23	4305.4
	LiP_5	$LiP_5 + 20\ O^{2-} \rightarrow 5PO_4^{3-} + Li^+ + 26\ e^-$	3.2	4299.5
	LiP_3	$LiP_3 + 12\ O^{2-} \rightarrow 3PO_4^{3-} + Li^+ + 16\ e^-$	3.14	4286.0

The traditional prelithiation agents are useful for addressing the lithium shortage, so that they compensate for the loss of electric quantity by employing equimolar active lithium sources (**Supplementary Table S1**). Take Li_5FeO_4 for an example, 4 Li^+ and 4 e^- can be released during the decomposition process. In the case of Li_xPPs, more electrons can be released during the oxidation process. In order to offset the electrons consumed by the reduction of electrolytes at the anode, more Li_5FeO_4 is needed compared with Li_xPPs.

Supplementary Table S2 Comparison of charge/discharge capacity of NCM811||Li half cell (the mass loading of NCM811 is 2.3±0.01 mg cm^{-2})

	Actual charging capacity (mAh)	Difference of their charging capacities (mAh)
Half cell using blank electrolyte	0.647	0.038
Half using Li_xPPs electrolyte	0.685	

Supplementary Table S3 The compensation capacity of Li_xPPs

Sample name	0.2 wt% Li_xPPs in 40 μl electrolyte
Total mass of Li_xPPs	0.0984 mg
Theoretical specific capacity of Li_xPPs based on electrons	4300 mAh/g
Theoretical compensation capacity based on electrons	0.423 mAh
Theoretical specific capacity of Li_xPPs based on Li^+	120 mAh/g
Theoretical compensation capacity based on Li^+	**0.0118** mAh

To demonstrate that the Li_xPPs functions via electron compensation rather than solely through lithium source compensation, we performed quantitative analysis using the initial charge curves of two NCM811 half cells with blank and Li_xPPs electrolytes. The fundamental principle of lithium source compensation is to employ the electrons generated concurrently with the extraction of lithium ions from materials in order to offset the initial irreversible losses within the battery. For example, in the case of LiP_7, if it serves solely as a lithium source, its capacity enhancement would be strictly limited by its stoichiometric lithium content (through the reaction of $LiP_7 \rightarrow Li^+ + P_7 + e^-$). The theoretical specific capacity of LiP_7 based on lithium extraction is approximately 120 mAh g^{-1}.

Comparing the NCM half cells employing 40 μL blank and Li_xPPs electrolytes, respectively, the initial charge curves demonstrate that the actual capacity enhancement measured in latter is 0.038 mAh (Supplementary Table S2). With a concentration of 0.2 wt% in electrolyte, the mass of Li_xPPs is 0.0984 mg in this cell (Supplementary Table S3). The theoretical capacity contribution attributable solely to lithium extraction by Li_xPPs is calculated to be 0.0118 mAh, while the theoretical compensable capacity, calculated based on electron contribution, is 0.423 mAh. The experimentally determined capacity enhancement significantly exceeds the theoretical upper limit achievable solely through lithium deintercalation processes. This finding provides strong evidence that Li_xPPs not only releases lithium ions at high potentials, but also undergoes further electrochemical oxidation of phosphorus species. The oxidation process provides additional electrons to the external circuit, thereby achieving "electronic compensation", which represents a 5.9% improvement in the total capacity of the NCM cathode.

1. Physical and chemical properties of Li_xPPs in ester-based electrolyte

Calculation of ΔE between P^0 and P^{5+}:

$P(s) + 4H_2O(l) \rightarrow H_3PO_4(s) + 5H^+(aq) + 5e^-$

ΔG=-163.812 kJ/mol ΔG=-nFE E=0.340 V

$2P(s) + 7H_2O(l) \rightarrow P_2O_7^{4-}(aq) + 14H^+(aq) + 10e^-$

ΔG=-258.952 kJ/mol ΔG=-nFE E=0.268 V

$P(s) + 4H_2O(l) \rightarrow H_2PO_4^-(aq) + 6H^+(aq) + 5e^-$

ΔG=-237.178 kJ/mol ΔG=-nFE E=0.3138 V

The ΔE between P^0 and P^{5+} is about 0.3 V, so the oxidation potential of Li_xPPs to P^{5+} is about 3.3 V vs. Li^+/Li, demonstrating that Li_xPPs can be oxidized to P^{5+} before the cut-off voltage of cathode.

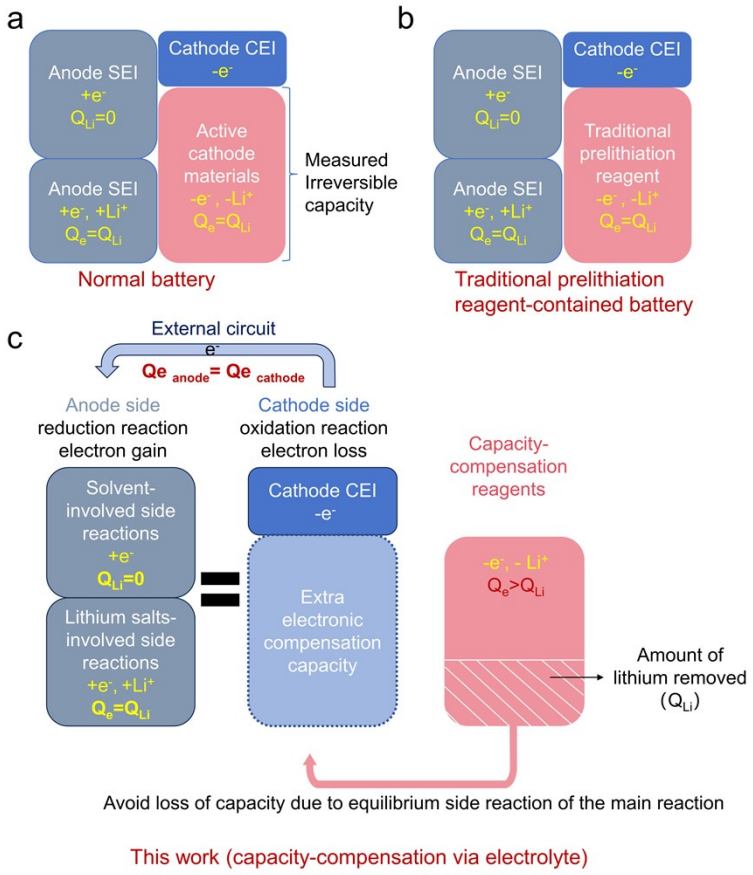

Supplementary Fig. 1. Schematic illustration of the initial side reactions and capacity-compensation mechanism in (a) normal battery, (b) traditional prelithiation reagent-contained battery and (c) this work (capacity-compensation via electrolyte).

In normal battery without prelithiation, the additional irreversible consumption of electrons and Li ions at the anode need to be balanced by active cathode materials, which provide the equimolar electrons and Li ions (**Supplementary Fig. 1(a)**). The mechanism of conventional prelithiation reagent is to extract lithium at a suitable potential that is below the high cut-off potential of cathode for charging (**Supplementary Fig. 1(b)**). Significantly, the traditional solid prelithiation reagents are only able to provide electrons that are equal to the molar amount of active Li^+ ions. Thus, a high proportion of prelithiation reagent is needed to compensate for the lack of electrons at the anode side, leading to the increase in the total electrode mass. In order to overcome the problem of traditional prelithiation reagents, we put forward the idea of capacity-compensation through electrolyte (**Supplementary Fig. 1(c)**). If the capacity-compensation additive can be dissolved in the solvent, it will not have adverse effects on the stability of the electrode and can achieve uniform

capacity compensation in the electrode. What's more, it will be compatible with the existing battery production process and there is not much safety concerns. Beyond that, if the reagent can provide more electrons than lithium ions, it will be more attractive due to the decreased lithium source cost. Importantly, the difference in principle of this work compared with the traditional solid-state prelithiation is that the total number of electrons to be compensated and the total number of Li ions to be compensated do not need to be equal.

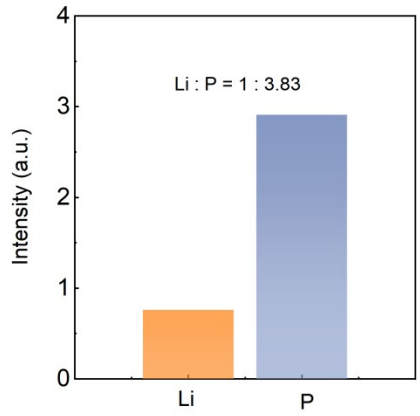

Supplementary Fig. 2. ICP of Li_xPPs in EC/DEC (1/1) solvent.

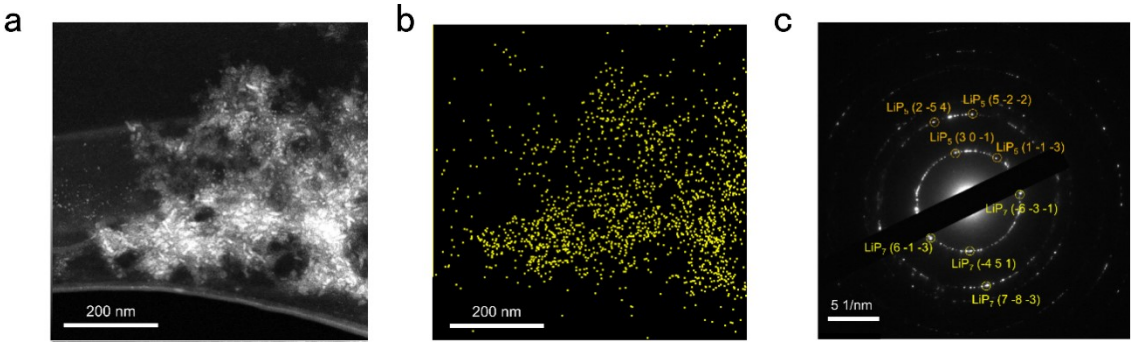

Supplementary Fig. 3. **a,** HAADF-STEM image of soluble Li_xPPs. **b,** Elemental mapping of P in soluble Li_xPPs. **c,** Selected area diffraction pattern of soluble Li_xPPs.

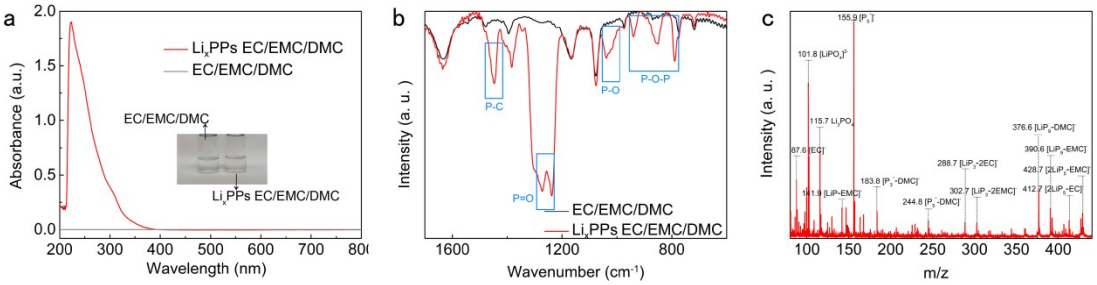

Supplementary Fig. 4. Characterization of LixPPs in EC/EMC/DMC (1/1/1) solvent. **a**, UV-vis spectrum, insets are the digital images of solutions. **b**, FT-IR spectra. **c**, Mass spectrum.

Li_xPPs can be dissolved in the solvent of EC/EMC/DMC as well (**Supplementary Fig. 4**), thus Li_xPPs can be dissolved in multiple solutions to serve as prelithiation additives in ester-based electrolytes for various battery systems. There is an obvious peak at 223.0 nm in UV band, indicating the component of Li_xPPs in EC/EMC/DMC solvent is different from that in EC/DEC (**Supplementary Fig. 4a**). The P-C, P=O and P-O and P-O-P bonds can also be identified in FT-IR spectra, and the mass spectrum shows the existence of P_3^-, P_5^-, LiP_5, LiP_9 and their solvated products in the solvent (**Supplementary Fig. 4b-c**).

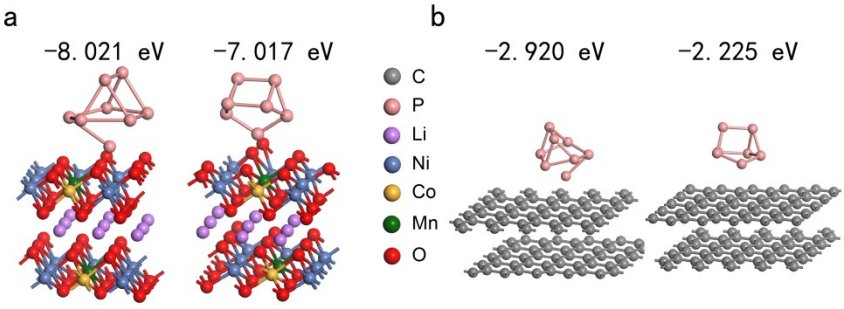

Supplementary Fig. 5. The structural representation for the adsorption of LiP_7 and P_7^- on NCM811 (**a**) and graphite (**b**).

2. Li_xPPs as prelithiation reagent in NCM811||graphite full cells

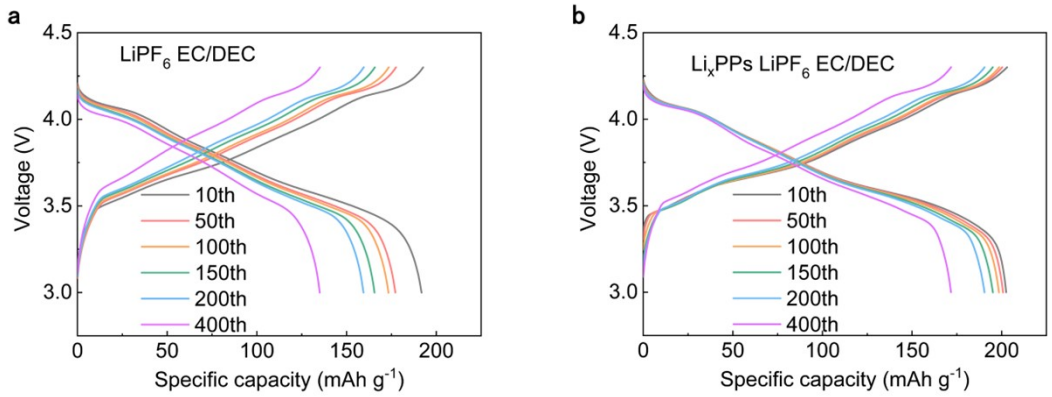

Supplementary Fig. 6. The charge and discharge curves of the 10th, 50th, 100th, 150th, 200th and 400th cycles at 100 mA g-1 in basic (**a**) and LixPPs-contained (**b**) electrolyte of NCM811||graphite full cells.

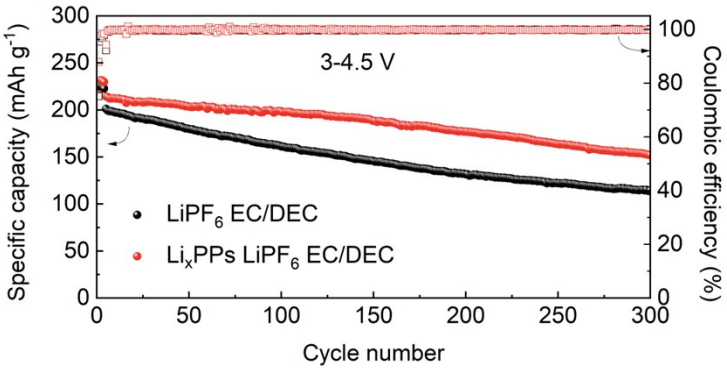

Supplementary Fig. 7. Cycling performance at 100 mA g^{-1} of NCM811||graphite full cells with a voltage range of 3-4.5 V.

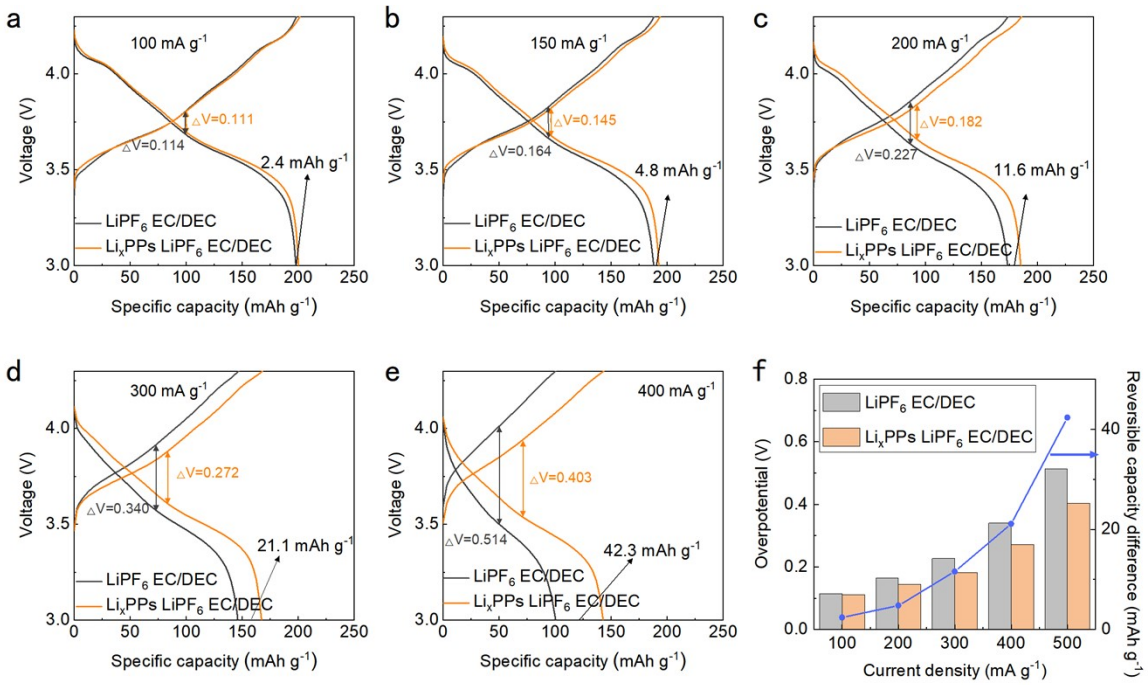

Supplementary Fig. 8. The charge and discharge curves of NCM811||graphite full cells at 100 (**a**), 150 (**b**), 200 (**c**), 300 (**d**), 400 (**e**) mA g^{-1} in basic and Li_xPPs-contained electrolyte. **f**, corresponding overpotentials and capacity difference at each current density.

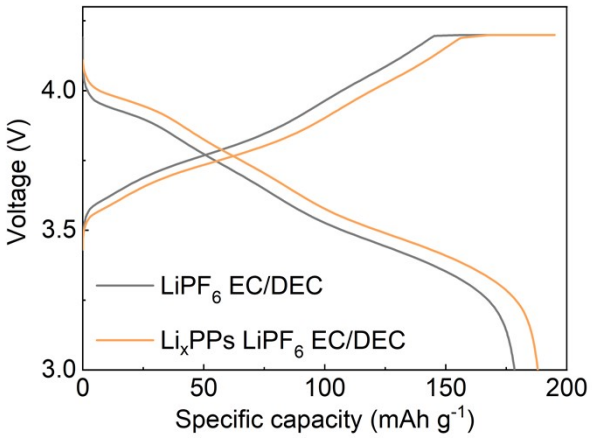

Supplementary Fig. 9. The initial galvanostatic charge and discharge curves for NCM811||graphite pouch cells (1.8 Ah).

3. Effect of the Li_xPPs additive on NCM811

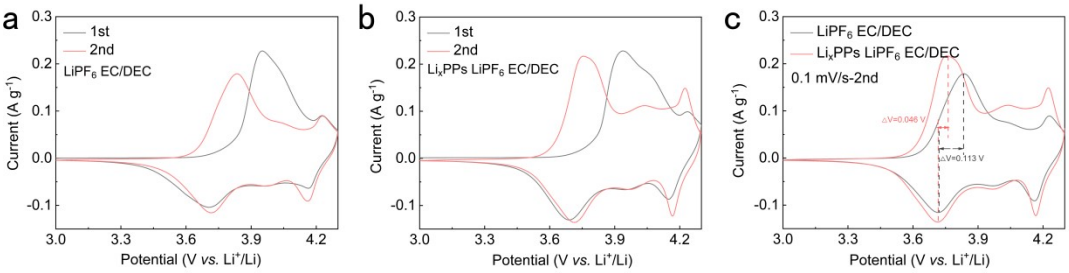

Supplementary Fig. 10. a, The 1st and 2nd cycles of CV plots for NCM811||Li cells containing basic electrolyte. **b,** The 1st and 2nd cycles of CV plots for NCM811||Li cells containing Li_xPPs-contained electrolyte. **c,** Comparison of the 2nd cycle of CV plots for NCM811||Li cells containing basic and Li_xPPs-contained electrolytes. All the CV tests are carried out at a scan rate of 0.1 mV/s.

During the second cycle, the increased peak area can also be observed in Li_xPPs-contained electrolyte, indicating the effect of capacity compensation (**Supplementary Fig. 10(c)**).

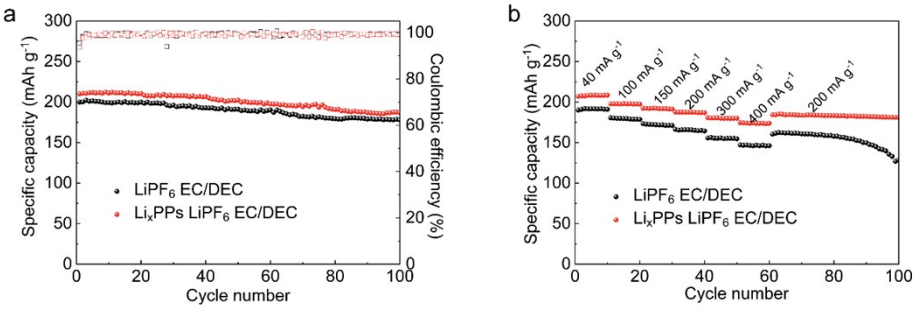

Supplementary Fig. 11. Electrochemical performances of NCM811||Li cells using the basic electrolyte and the Li_xPPs-contained electrolyte, respectively. a, Cycling performance at 40 mA g^{-1}. b, Rate performances.

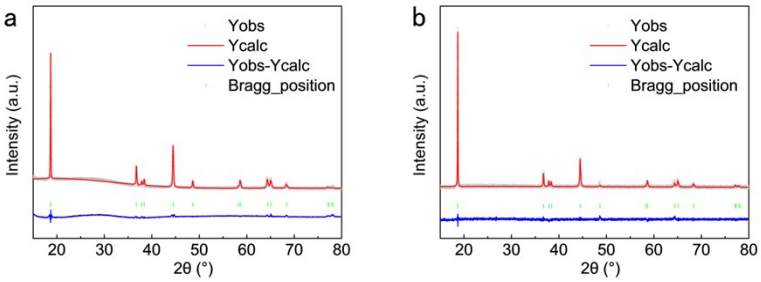

Supplementary Fig. 12. The Rietveld refinement results for NCM811 cycled for 20 cycles in basic (**a**) and Li_xPPs-contained (**b**) electrolytes.

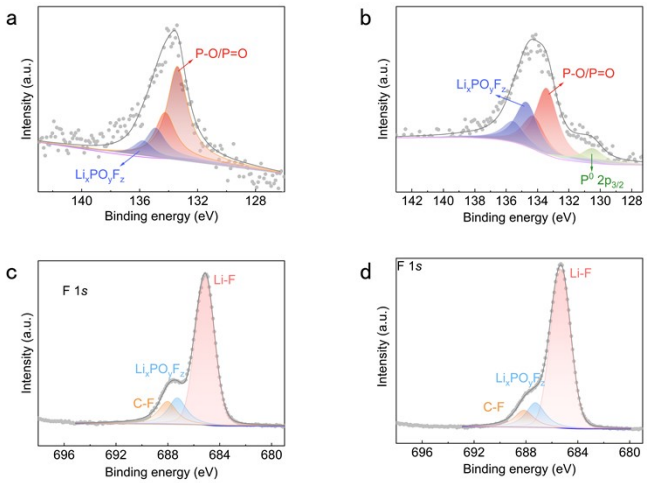

Supplementary Fig. 13. High-resolution XPS spectra of NCM811 electrode after 20 cycles at 100 mA g^{-1} with blank electrolyte of P 2p (**a**), F 1s (**c**). High-resolution XPS spectra of NCM811 electrode after 20 cycles at 100 mA g^{-1} with Li_xPPs-contained electrolyte of P 2p (**b**), F 1s (**d**).

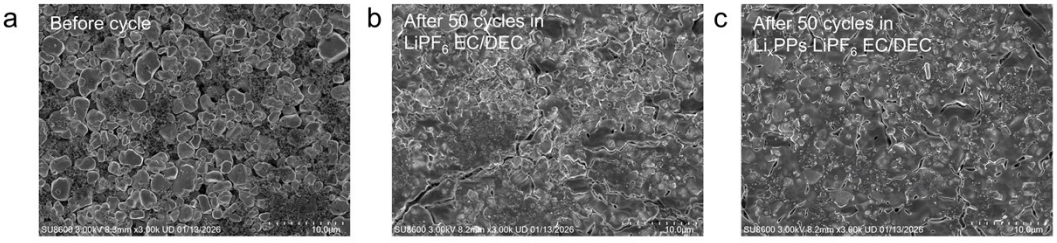

Supplementary Fig. 14. SEM images of the NCM811 cathode after 50 cycles in (**a**) $LiPF_6$ EC/DEC and (**b**) Li_xPPs $LiPF_6$ EC/DEC.

As shown in Supplementary Fig. 14a, the pristine NCM exhibits a typical and intact spherical morphology before cycling. After 50 cycles in the blank electrolyte ($LiPF_6$ EC/DEC), the surface morphology of the electrode deteriorated significantly (Supplementary Fig. 14b). The NCM

particle surface was completely covered by a thick and uneven layer of substances, causing the original boundaries between particles to become blurred, accompanied by severe cracks. This pasty surface morphology suggests the significant oxidative decomposition side reactions took place between the high-voltage cathode and the electrolyte. Consequently, the disordered accumulation of a large quantity of decomposition products, such as lithium alkyl carbonates, occurred on the electrode surface, leading to the formation of a high-impedance and structurally unstable CEI.

In contrast, after 50 cycles in an electrolyte containing the Li_xPPs additive (Supplementary Fig. 14c), the NCM electrode surface exhibits a markedly distinct morphology. While a CEI is also observed to cover the surface, this layer is evidently thinner, more compact, and more uniform in nature. These findings provide strong evidence that Li_xPPs molecules undergo preferential oxidation at the cathode surface, thereby facilitating the formation of a stable and thin interfacial protective CEI. The CEI effectively prevents direct contact between the active material and the electrolyte, significantly inhibiting the ongoing oxidative decomposition of the electrolyte and thus maintaining the structural stability of the cathode material.

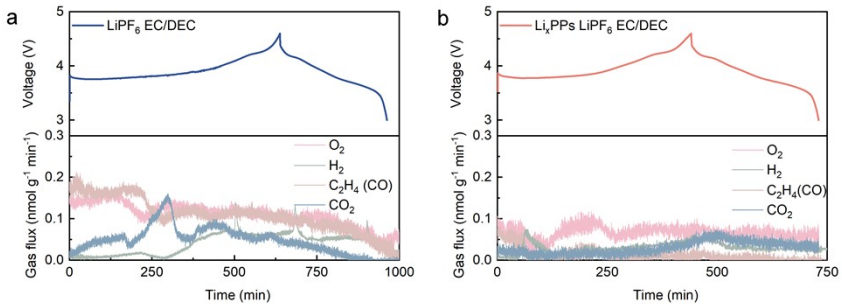

Supplementary Fig. 15. First charge/discharge potential curves, and corresponding gas evolution profiles of NCM811 half-cells with (**a**) the reference electrolyte ($LiPF_6$ EC/DEC (1/1)) and the (**b**) Li_xPPs-based electrolyte cycled in the voltage range of 3~4.6 V at a rate of 0.1C and room temperature.

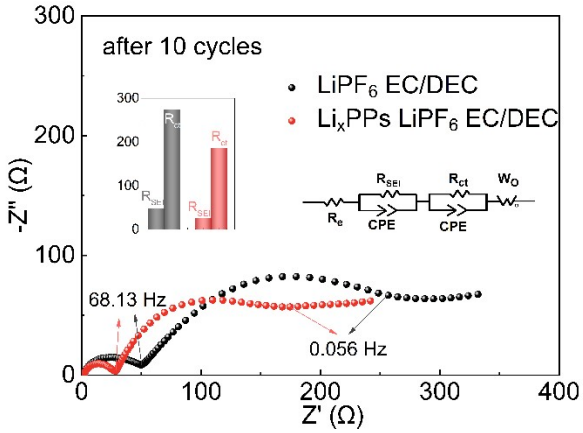

Supplementary Fig. 16. EIS spectra of NCM811 after 10 cycles at 100 mA g^{-1} with basic and Li_xPPs-contained electrolyte.

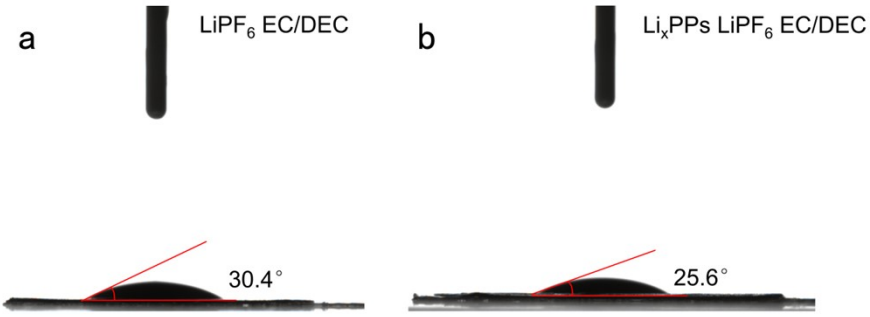

Supplementary Fig. 17. Contact angles of basic (a) and Li_xPPs-contained (b) electrolytes on graphite electrodes.

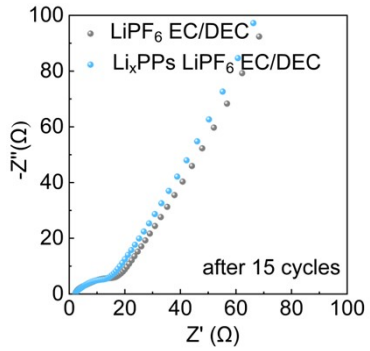

Supplementary Fig. 18. EIS spectra of graphite||Li half cells after15 cycles.

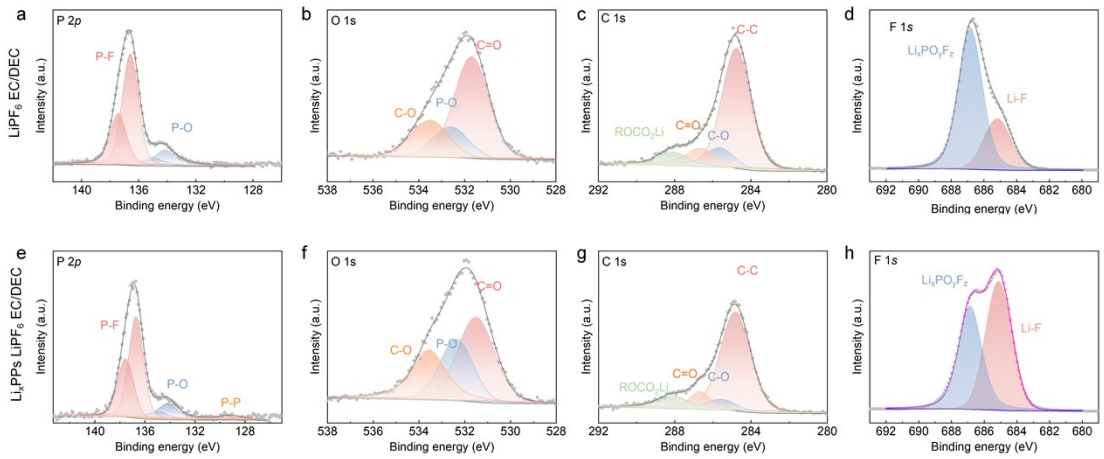

Supplementary Fig. 19. High-resolution XPS spectra of P 2p for graphite electrodes after 20 cycles at 0.5 C with (**a**) blank and (**e**) Li_xPPs-contained electrolytes. XPS spectra of O 1s for (**b**) blank and (**f**) Li_xPPs-contained electrolytes. XPS spectra of C 1s for (**c**) blank and (**g**) Li_xPPs-contained electrolytes.High-resolution XPS spectra of F 1s for graphite electrodes after 20 cycles at 0.5 C with (**d**) blank and (**h**) Li_xPPs-contained electrolytes.

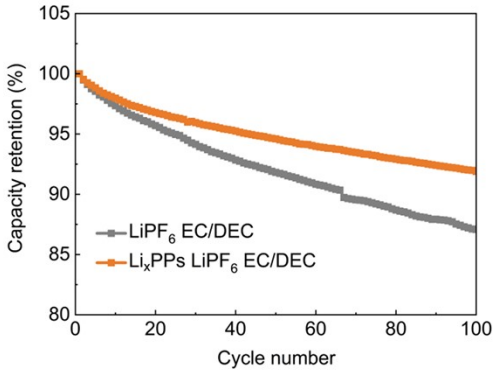

Supplementary Fig. 20. The electrochemical cycling performances of NCM811||SiO_x-C pouch cells (1 Ah) at 1C with a voltage range of 3-4.2 V.

In order to verify the influence of Li_xPPs-based electrolyte on other anodes, NCM||SiO_x-C pouch cells were evaluated. As shown in Supplementary Fig. 20, the capacity retention of the full cell using Li_xPPs-based electrolyte after 100 cycles is 92.0%, higher than the control sample (87.1%). Therefore, Li_xPPs are compatible with SiO_x anodes. The key reasons behind the non-enhancement of capacity in full cells featuring SiO_x anodes stem from two principal factors: (1) The proliferation

of undesired side reactions involving the SiO_x anode, and (2) The increased tendency of Li_xPPs to adsorb and react on the surface of SiO_x, subsequently diminishing their positive impact on the cathode's overall capacity.